Carbon-Sulfur Bond Strength in Methanesulfinate and Benzenesulfinate Ligands Directs Decomposition of Np(V) and Pu(V) Coordination Complexes

Valérie Vallet, Yu Gong, Mohammad Saab, Florent Réal, John Gibson

Carbon-Sulfur Bond Strength in Methanesulfinate and Benzenesulfinate Ligands Directs Decomposition of Np(V) and Pu(V) Coordination Complexes

Valérie Vallet[a,*], Yu Gong[b], Mohamad Saab[a], Florent Réal[a], John K. Gibson[b,*]

[a]Univ. Lille, CNRS, UMR 8523 - PhLAM - Physique des Lasers Atomes et Molécules, F-59000 Lille, France

[b]Chemical Sciences Division, Lawrence Berkeley National Laboratory, Berkeley, California 94720, United States

[*]Corresponding authors: valerie.vallet@univ-lille.fr; jkgibson@lbl.gov

Abstract

Gas-phase coordination complexes of actinyl(V) cations, AnO_2^+, provide a basis to assess fundamental aspects of actinide chemistry. Electrospray ionization of solutions containing an actinyl cation and sulfonate anion $CH_3SO_2^-$ or $C_6H_5SO_2^-$ generated complexes $[(An^VO_2)(CH_3SO_2)_2]^-$ or $[(An^VO_2)(C_6H_5SO_2)_2]^-$ where An = Np or Pu. Collision induced dissociation resulted in C-S bond cleavage for methanesulfinate to yield $[(An^VO_2)(CH_3SO_2)(SO_2)]^-$, whereas hydrolytic ligand elimination occurred for benzenesulfinate to yield $[(An^VO_2)(C_6H_5SO_2)(OH)]^-$. These different fragmentation pathways are attributed to a stronger C_6H_5-SO_2^- versus CH_3-SO_2^- bond, which was confirmed for both the bare and coordinating sulfinate anions by energies computed using a relativistic multireference perturbative approach (XMS-CASPT2 with spin-orbit coupling). The results demonstrate shutting off a ligand fragmentation channel by increasing the strength of a particular bond, here a sulfinate C-S bond. The $[(An^VO_2)(CH_3SO_2)(SO_2)]^-$ complexes produced by CID spontaneously react with O_2 to eliminate SO_2, yielding $[(AnO_2)(CH_3SO_2)(O_2)]^-$, a process previously reported for An = U and found here for An = Np and Pu. Computations confirm that the O_2/SO_2 displacement reactions should be exothermic or thermoneutral for all three An, as was experimentally established. The computations furthermore reveal that the products are superoxides $[(An^VO_2)(CH_3SO_2)(O_2)]^-$ for An = Np and Pu, but peroxide $[(U^{VI}O_2)(CH_3SO_2)(O_2)]^-$. Distinctive reduction of O_2^- to O_2^{2-} concomitant with oxidation of U(V) to U(VI) reflects the relatively higher stability of hexavalent uranium versus neptunium and plutonium.

Introduction

Sulfinate anions with general formula RSO_2^-, where R is an organic group, are conjugate bases of sulfinic acids, RSO_2H. Cleavage of the sulfinate carbon-sulfur bond provides a radical $R^\bullet$ fragment, which can engage in reactions such as carbon-carbon coupling. This and other types of C-S bond cleavages and C-C couplings are usually accomplished using a metal catalyst (M) to yield a C-M-S intermediate, with mechanistic details typically remaining elusive.[1] A useful prelude to directly probing actual catalytic systems is to examine related processes in simple gas-phase coordination complexes having ligands like sulfinate tethered to a metal center.[2] Specifically, anion complexes $[M(L)_n]^-$ formally having a metal cation, $M^{(n-1)+}$, coordinated by n anion ligands, L^-, are well suited for study by electrospray ionization (ESI) coupled to quadrupole ion trap mass spectrometry (QIT-MS), a gas-phase technique that has appropriately been termed "a complete chemical laboratory".[3] In QIT-MS, ligand cleavage is accomplished by low-energy collision induced dissociation (CID) in which the internal energy of the complex is gradually increased to above its fragmentation threshold.[4] The observed fragmentation pathway(s) reflect the underlying potential energy surface (PES), which includes the overall reaction energy as well as transition state barriers that may inhibit fragmentation and control kinetics. For relatively small isolated gas-phase complexes it is often feasible to reliably compute relevant energy surfaces for unimolecular CID processes to rationalize observations and understand underlying and related phenomena.[5,6]

O'Hair and co-workers used CID to study the competition between decomposition of methanesulfinate and acetate ligands coordinated to copper in the gas-phase complex $[Cu(CH_3SO_2)(CH_3CO_2)]^-$.[7] The favored CID pathway was C-S cleavage with SO_2 eliminated to yield organocuprate complex $[Cu(CH_3CO_2)(CH_3)]^-$; alternative C-C cleavage with CO_2 elimination was not observed. Curiously, DFT calculations indicated that the lowest energy decomposition pathway is loss of CO_2 (ΔH = 68 kJ/mol), rather than the observed loss of SO_2 (ΔH = 108 kJ/mol). However, the computed PES revealed the origins of the favored CID pathway as a lower transition state barrier for SO_2 elimination, which results in kinetic rather than thermodynamic control of this particular dissociation. The O'Hair group recently employed CID and DFT to evaluate decomposition of gas-phase palladium benzenesulfinate complexes, with a focus on comparison with the corresponding carboxylates.[8] In that work, CID resulted in elimination of SO_2 with formation of a Pd-C_6H_5 organometallic bond, exhibiting chemistry reminiscent of the Cu-CH_3 situation.

Our earlier foray into sulfinate complexes employed the uranyl(V) cation, UO_2^+, coordinated by two methanesulfinate ligands in $[(UO_2)(CH_3SO_2)_2]^-$.[9] CID resulted in C-S bond cleavage with CH_3

elimination to yield $[(UO_2)(CH_3SO_2)(SO_2)]^-$ comprising a sulfur dioxide anion ligand. Retention of the SO_2 fragment, rather than CH_3 as was previously observed for copper, reflects the more oxophilic character of actinides in general and uranium in particular.[10] It was additionally found that the uranyl(V) CID product spontaneously reacts with O_2, with elimination of SO_2 to yield $[(UO_2)(CH_3SO_2)(O_2)]^-$. Reasonable assignments of the nature of this latter reaction product include superoxide O_2^- ligand with retention of oxidation state U(V), and peroxide O_2^{2-} ligand with oxidation to U(VI). DFT computations indicate the latter, implying oxidation of uranyl(V) to uranyl(VI) upon replacement of SO_2 by O_2. We here extend this general line of inquiry farther into the actinide series with a study of methanesulfinate complexes of neptunyl(V) and plutonyl(V). It was here found that CID of both of the $[(AnO_2)(CH_3SO_2)_2]^-$ (An = Np and Pu) results in CH_3 elimination, as we previously reported for An = U. Furthermore, CID products $[(AnO_2)(CH_3SO_2)(SO_2)]^-$ spontaneously react with O_2 to eliminate SO_2 and afford $[(AnO_2)(CH_3SO_2)(O_2)]^-$, as was also previously observed for the corresponding uranium complex. However, DFT computations indicate that the products are neptunyl(V) and plutonyl(V) superoxides. This contrast to formation of a uranyl(VI) peroxide reflects the diminishing stability beyond uranyl of actinyl(VI) relative to actinyl(V).[11]

A focus of our renewed interest in sulfinate complexes was to explore rational and predictable control of ligand decomposition in CID, and by inference also in condensed phases. The hypothesis was that for two organosulfinate ligands, $R^1SO_2^-$ and $R^2SO_2^-$, the transition state barriers to C-S bond cleavage should correlate with the net energy for this dissociation. The rationale for this premise is essentially Hammond's Postulate.[12] In particular, as analogous C-S bond cleavage mechanisms are generally expected for different RSO_2^- ligands, the transition states should be comparable. Furthermore, as is typical for such endothermic bond cleavage reactions the pertinent transition state should resemble the products R and SO_2^- more so than the R-SO_2^- reactant. According to Hammond's Postulate, as the reaction becomes increasingly endothermic—i.e. the products become higher energy reflecting higher bond dissociation energy (BDE)—the corresponding transition state reaction barrier should similarly increase in energy. As exemplary ligands to test this simple premise with a specific comparison, we identified two elementary organosulfinates, methanesulfinate ($CH_3SO_2^\bullet$) and benzenesulfinate ($C_6H_5SO_2^\bullet$). The expectation was that the C-S bond would be weaker in the former than in the latter, such as it for methanethiol (BDE = 308 kJ mol^{-1}) versus benzenethiol (BDE = 366 kJ mol^{-1}), as well as for other CH_3-X versus C_6H_5-X bonds (X = halide, NO_2, OH, H, CH_3 etc.).[13] We here first report on a computational study of neutral CH_3SO_2 and $C_6H_5SO_2$, and anions $CH_3SO_2^-$ and $C_6H_5SO_2^-$, to establish their structures and energetics. We then report CID results for $An^VO_2(CH_3SO_2)_2^-$ and $An^VO_2(C_6H_5SO_2)_2^-$ (An = Np, Pu), with observation of C-S

fragmentation for the methanesulfinate, versus reaction with water and elimination of a protonated ligand for benzenesulfinate. We finally present computations that rationalize the experimental observations.

Computational Details

All geometries were optimized using the PBE0 functional of the density, followed by a harmonic vibrational frequency calculation using the Turbomole package.[1] The sum of the partition functions for the translational, rotational and harmonic vibrational motions is used to compute the contributions to the enthalpies and free energies. All atoms are described with aug-cc-pVTZ triple zeta quality basis sets,[14] while the actinides are described by a small-core (32 valence electrons) relativistic pseudopotential,[15] with the corresponding segmented basis sets with quadruple zeta quality.[16] Single-point electronic energy calculations on $CH_3SO_2^{\bullet}$, $C_6H_5SO_2^{\bullet}$ and their anion counterparts were performed with the MP2 and CCSD(T) methods, with the MOLPRO package,[17] with the reference and correlation energies extrapolated to the complete basis set limit (CBS) with the two-point (triple and quadruple-zeta) extrapolation formulas.[18-20]

To accurately treat the open-shell character of the actinyl complexes in their hexavalent or pentavalent state, as well as the radical molecules such as $CH_3^{\bullet}$, state-averaged CASSCF (complete-active-space self-consistent field) relativistic calculations were performed with the OpenMolcas program.[21] These calculations used the second-order Douglas-Kroll-Hess scalar relativistic Hamiltonian[22] and all-electron atomic natural orbitals relativistically correlation consistent basis sets[23,24] with triple-ζ quality. Expanding the basis set quality to quadruple-ζ only leads to changes of a few kJ mol^{-1} for the computed enthalpies of reaction. For the actinyl complexes, the zeroth-order CASSCF wave function includes all possible configurations with from one up to three unpaired electrons occupying the four non-bonding f_δ and f_φ orbitals localized on the actinyl(V) unit, along with one electron on the SO_2^- radical unit, for the $[AnO_2(CH_3SO_2)(SO_2)]^-$ and $[AnO_2(C_6H_5SO_2)(SO_2)]^-$ molecules, or one electron on the O_2^- superoxo radical for the $[AnO_2(CH_3SO_2)(O_2)]^-$ and $[AnO_2(C_6H_5SO_2)(O_2)]^-$. For the small radical molecules, the active spaces are generated out of the valence shell orbitals. Dynamic correlation of the valence electrons was included via extended multi-state complete active space second-order perturbation theory (XMS-CASPT2).[25] The resulting XMS-CASPT2 wave-functions computed for all relevant multiplicities are coupled by spin-orbit coupling using the RASSI formalism[26] and atomic mean-field spin-orbit integrals,[27] to yield the SO-XMS-CASPT2 energies. The spin-orbit ground-state wave-functions were analyzed by computing natural spin orbitals (NSOs),[28,29] $\varphi_p^z(r)$, as eigenvalues of the spin

magnetization density matrix $m_z(r)$, along the z-actinyl axis. The isosurfaces were drawn with the AIMAll program.[30]

For each actinyl complex, we explored several ground-state electronic configurations corresponding to different ground-state multiplicities at the PBE0 level of theory. The most stable configurations reported in Table 4 were confirmed by the XMS-CASPT2 calculations. For uranyl, the results agree with those previously obtained using the B3LYP functional.[9]

Experimental Details

Caution – The Np-237 and Pu-242 isotopes employed in this work are radioactive and must be handled using appropriate precautions in special radiological laboratories.

The experiments employed an Agilent 6340 QIT-MS, with the ESI source in a radiological containment glove box.[31] Complexes $[AnO_2(RSO_2)_2]^-$ (An = Np or Pu; R = CH_3 or C_6H_5) were produced by ESI of methanol (with 10% water) solutions of $An^{VI}O_2(ClO_4)_2$ and RSO_2Na (An:R = 1:5 - 1:10, 0.2 mM An) . The employed isotopes, Np-237 and Pu-242, undergo alpha-decay with half-lives of 2.1×10^6 y and 3.8×10^5 y, respectively. The MS^n capabilities of the QIT/MS enables multiple (n) sequential mass spectrometry stages, in each of which ions having a particular mass-to-charge ratio, m/z, are isolated and subjected to either CID—i.e. excitation and energetic collisions with helium—or low-energy (T ≈ 300 K[32]) ion-molecule reactions (IMRs) with gases in the ion trap. Ion intensity distributions are dependent on instrumental parameters, particularly the ion trap RF voltage; the employed parameters are similar to those used previously.[9] High-purity nitrogen gas for nebulization and drying in the ion transfer capillary was boil-off from liquid nitrogen. The He buffer gas pressure in the ion trap is ~10^{-4} Torr, and background H_2O and O_2 are both present at ~10^{-6} Torr.[33,34]

Results and Discussion

Computed structures and energies of CH_3SO_2 and $C_6H_5SO_2$

Association reactions (1) and (2) were assessed with a primary goal of quantifying the C-S bond strengths in $CH_3SO_2^{\bullet}$ and $C_6H_5SO_2^{\bullet}$.

$$CH_3^{\bullet} + SO_2 \rightarrow CH_3SO_2^{\bullet} \quad (1)$$

$$C_6H_5^{\bullet} + SO_2 \rightarrow C_6H_5SO_2^{\bullet} \quad (2)$$

Quantum chemical (DFT, MP2 and CCSD(T)) calculations on $CH_3SO_2^{\bullet}$ by Li et al.[35] previously revealed that among thirteen identified isomers, $CH_3SO_2^{\bullet}$, *cis*-$CH_3OSO^{\bullet}$ and *trans*-$CH_3OSO^{\bullet}$ are the most stable. The structures, which are shown for the corresponding anions in Figure 1, feature a C-SO_2 connectivity for $CH_3SO_2^{\bullet}$, while C-OSO for the other two. We considered for $C_6H_5SO_2^{\bullet}$ the corresponding

isomers denoted $C_6H_5SO_2^{\bullet}$ and $C_6H_5OSO^{\bullet}$ where the latter corresponds to both "*cis*-$C_6H_5OSO^{\bullet}$" and "*trans*-$C_6H_5OSO^{\bullet}$" as they are identical in this case. Specifically considered were reactions 3-7 for the neutrals and, given our particular interest in anion ligands, corresponding reactions 3a-7a for the anionic species. Note that reaction 3 is the same as 1, and 6 is the same as 2, with these duplications for clarity.

$CH_3^{\bullet} + SO_2 \rightarrow CH_3SO_2^{\bullet}$ / $CH_3 + SO_2^{-} \rightarrow CH_3SO_2^{-}$ (3) / (3a)

$CH_3^{\bullet} + SO_2 \rightarrow$ *cis*-$CH_3OSO^{\bullet}$ / $CH_3 + SO_2^{-} \rightarrow$ *cis*-CH_3OSO^{-} (4) / (4a)

$CH_3^{\bullet} + SO_2 \rightarrow$ *trans*-$CH_3OSO^{\bullet}$ / $CH_3 + SO_2^{-} \rightarrow$ *trans*-CH_3OSO^{-} (5) / (5a)

$C_6H_5^{\bullet} + SO_2 \rightarrow C_6H_5SO_2^{\bullet}$ / $C_6H_5 + SO_2^{-} \rightarrow C_6H_5SO_2^{-}$ (6) / (6a)

$C_6H_5^{\bullet} + SO_2 \rightarrow C_6H_5OSO^{\bullet}$ / $C_6H_5 + SO_2^{-} \rightarrow C_6H_5OSO^{-}$ (7) / (7a)

Table 1. Computed enthalpies ΔH_r and Gibbs free energies ΔG_r at 298.15 K in kJ mol^{-1} for neutral reactions 3 - 7.

	ΔH_r			ΔG_r		
Reaction	PBE0	MP2 (CBS)	CCSD(T) (CBS)	PBE0	MP2 (CBS)	CCSD(T) (CBS)
(3)	-90.6	-75.3	-69.6	-47.5	-32.1	-26.4
(4)	-114.4	-81.7	-84.6	-75.7	-42.9	-45.9
(5)	-105.7	-70.8	-74.0	-68.9	-33.7	-36.9
(6)	-129.0	-134.1	-118.0	-79.1	-84.1	-68.1
(7)	-169.6	-153.9	-145.9	-124.9	-109.2	-101.2

Table 2. Computed enthalpies ΔH_r and Gibbs free energies ΔG_r at 298.15 K in kJ mol^{-1} for anion reactions 3a - 7a.

	ΔH_r			ΔG_r		
Reaction	PBE0	MP2(CBS)	CCSD(T) (CBS)	PBE0	MP2(CBS)	CCSD(T) (CBS)
(3a)	-178.5	-200.1	-198.0	-134.5	-156.1	-154.0
(4a)	-75.9	-70.0	-80.3	-35.2	-29.4	-39.6
(5a)	-58.8	-50.2	-60.2	-22.2	-13.6	-23.6
(6a)	-231.5	-278.5	-236.6	-182.0	-229.0	-214.0
(7a)	-180.9	-192.5	-190.7	-131.7	-143.3	-141.5

The neutral results in Table 1 reveal that for all employed levels of theory, and considering both enthalpy and free energy, the reactions are most exothermic for formation of *cis*-$CH_3OSO^{\bullet}$ (reaction 4) and $C_6H_5OSO^{\bullet}$ (reaction 7), which indicates that these are the most stable configurations of the neutral molecules. In contrast, the anion results in Table 2 show that the reactions are most exothermic for

formation of $CH_3SO_2^-$ (reaction 3a) and $C_6H_5SO_2^-$ (reaction 6a). The substantial shift in isomer stability from neutral to anion largely reflects the higher electron affinity of oxygen versus sulfur, which favors R-OSO$^\bullet$ in the neutrals whereas R-SO_2^- in the anions. At all three levels of theory employed for the neutrals, for the most stable structure the BDE[C_6H_5-OSO$^\bullet$] (from reaction 7) is greater than BDE[CH_3-OSO$^\bullet$] (from reaction 4) by more than 50 kJ mol^{-1}. At the PBE0, MP2(CBS) and CCSD(T)(CBS) levels used for both anionic species, for the most stable structure the BDE[C_6H_5-SO_2^-] (from reaction 6a) is greater than BDE[CH_3-SO_2^-] (from reaction 3a), also by more than 50 kJ mol^{-1}. As was expected based on other types of molecules, both the C_{phenyl}-O and C_{phenyl}-S bonds are substantially stronger than the corresponding C_{methyl}-O and C_{methyl}-S bonds.

The relative energies of the anion isomers are summarized in Table 3, with the corresponding structures shown in Figure 1. Given the clearly higher stabilities of anion isomers $CH_3SO_2^-$ and $C_6H_5SO_2^-$ with C-SO_2 connectivities, only these structures are considered below for sulfinate ligands bound to actinyl cations. If these RSO_2 were somehow to serve as neutral ligands, then the lowest energy ligand structures should instead have an R-OSO connectivity. It is however doubtful that interconversion between the two isomeric structures is facile. Because the experiments here employed sodium sulfinates, RSO_2Na, as the ligand sources, the ligands can confidently be considered as anionic R-SO_2^- based on both thermodynamic and kinetic considerations.

Table 3. Energies ΔE and Gibbs free energies ΔG at 298.15 K in kJ mol^{-1} relative to the most stable isomers $CH_3SO_2^-$, and $C_6H_5SO_2^-$ computed at the PBE0, MP2(CBS) and CCSD(T) levels.

	PBE0	MP2 (CBS)	CCSD(T) (CBS)	PBE0	MP2 (CBS)	CCSD(T) (CBS)
$CH_3SO_2^-$	0.0	0.0	0.0	0.0	0.0	0.0
cis-CH_3OSO^-	100.7	128.3	115.9	99.2	126.8	114.4
trans-CH_3OSO^-	118.5	148.7	136.6	112.3	142.6	130.4
$C_6H_5SO_2^-$	0.0	0.0	0.0	0.0	0.0	0.0
$C_6H_5OSO^-$	51.2	86.7	73.5	50.3	85.7	72.5

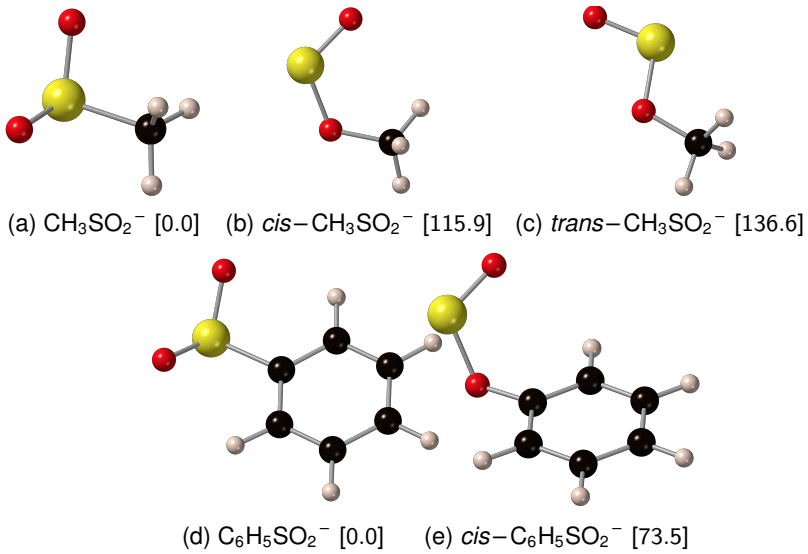

Figure 1. Perspective views of the most stable isomers of $CH_3SO_2^-$ and $C_6H_5SO_2^-$, with relative energies ΔE, in kJ mol^{-1}, computed at the CCSD(T)(CBS) level of theory in square brackets.

Chemistry of $[AnO_2(CH_3SO_2)_2]^-$ and $[AnO_2(C_6H_5SO_2)_2]^-$ (An = Np, Pu)

Collision induced dissociation and ion-molecule reactions

Experimental results for sulfinate complexes of An = Np and Pu are shown in Figures 2-4. The results for the An = Np and the corresponding An = Pu complexes are essentially the same. From Figure 2 it is apparent that the primary CID reaction for $[AnO_2(CH_3SO_2)_2]^-$ is elimination of CH_3 to yield $[AnO_2(CH_3SO_2)(SO_2)]^-$ as given by reaction (8). Also apparent in Figure 2 is a small peak that corresponds to replacement of SO_2 by O_2 that is inherently present as a background gas, i.e. reaction (9). Reaction of isolated $[AnO_2(CH_3SO_2)(SO_2)]^-$ with background gases at T~300 K—results shown in Figure 3—confirm that ion-molecule reaction (9) is exothermic and occurs spontaneously under these low-energy conditions. The CID results for $[AnO_2(C_6H_5SO_2)_2]^-$ in Figure 4 indicate reaction (11) as the dominant pathway, which is very different from the ligand cleavage seen for $[AnO_2(CH_3SO_2)_2]^-$. In particular, reaction (10), which is the analog of reaction (8), was not observed. The reactant water molecule that appears in CID reaction (10) is present as a background gas in the ion trap, like the O_2 reagent that is manifested in the results in Figure 3 and appears in reaction (9).

$$[AnO_2(CH_3SO_2)_2]^- \rightarrow [AnO_2(CH_3SO_2)(SO_2)]^- + CH_3^{\bullet} \qquad (8)$$

$$[AnO_2(CH_3SO_2)(SO_2)]^- + O_2 \rightarrow [AnO_2(CH_3SO_2)(O_2)]^- + SO_2 \quad (9)$$

$$[AnO_2(C_6H_5SO_2)_2]^- \rightarrow [AnO_2(C_6H_5SO_2)(SO_2)]^- + C_6H_5^{\bullet} \quad (10)$$

$$[AnO_2(C_6H_5SO_2)_2]^- + H_2O \rightarrow [AnO_2(C_6H_5SO_2)(OH)]^- + C_6H_5SO_2H \quad (11)$$

The CID results are in accord with the simple motivating predictions outlined above. In particular, it was expected that the CH_3-SO_2 bond would be weaker and thus both thermodynamically and kinetically more susceptible to cleavage than the C_6H_5-SO_2 bond. The computational results presented above confirm that the C-S bond in methanesulfinate anion is substantially weaker than that in benzenesulfinate anion. The CID results confirm that methanesulfinate C-S cleavage reaction (8) is observed whereas benzenesulfinate C-S cleavage reaction (10) is not. Described below are computational assessments of these reactions and the species involved. Also computationally assessed are observed reactions (9) and (11), with focus on the overall energetics and the nature of the products $[AnO_2(CH_3SO_2)(O_2)]^-$ and $[AnO_2(C_6H_5SO_2)(OH)]^-$. Because reactions (8) and (9) were previously also reported for An = U,[9] computations were likewise performed for the related uranium complexes along with those of neptunium and plutonium that were the focus of the experiments reported here.

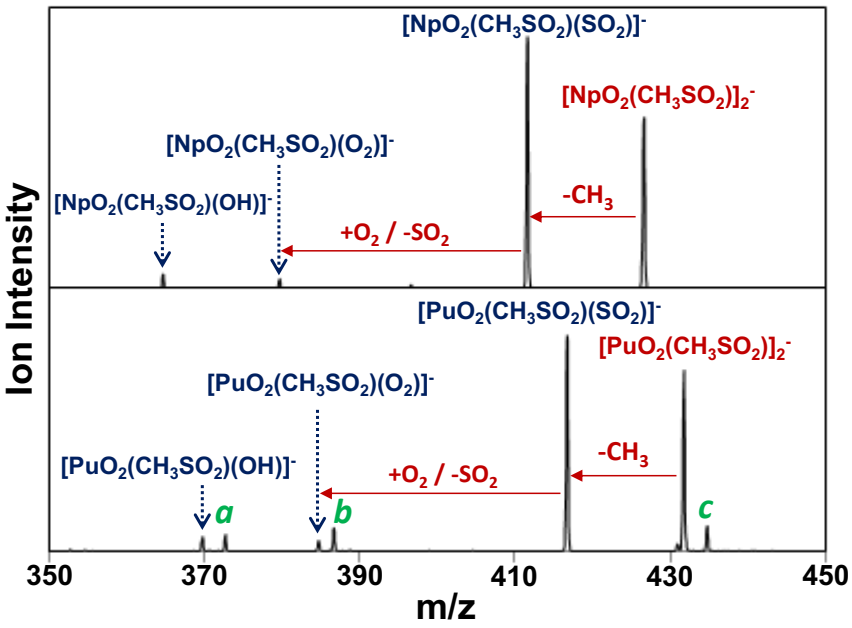

Figure 2. CID mass spectra for $[NpO_2(CH_3SO_2)_2]^-$ (top) and $[PuO_2(CH_3SO_2)_2]^-$ (bottom) with primary CH_3 eliminations and secondary reactions with O_2 as indicated. Also identified are sulfinate hydroxides; and ***a*** $[PuO_2(SO_2)(OH)(H_2O)]^-$, ***b*** $[PuO_2(SO_2)(O_2)(OH)]^-$, and ***c*** $[PuO_2(CH_3SO_2)(SO_2)(H_2O)]^-$.

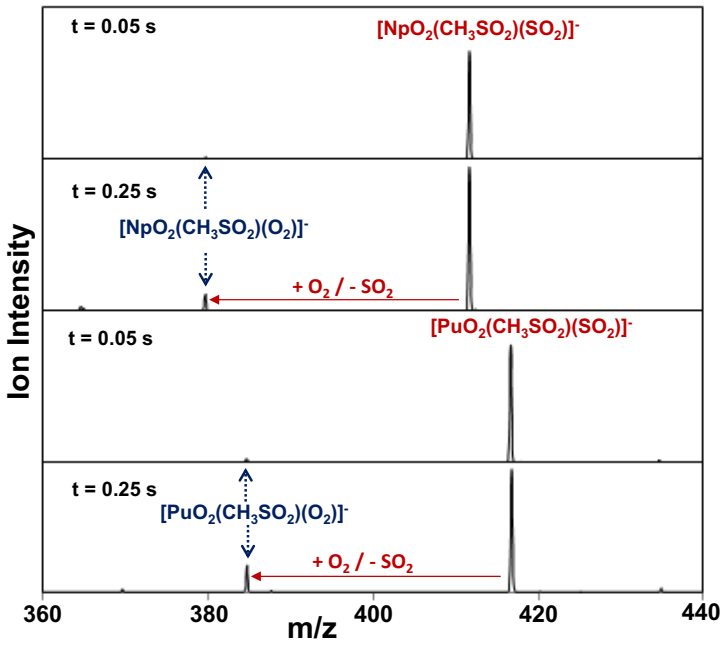

Figure 3. Mass spectra acquired after reactions of $[NpO_2(CH_3SO_2)(SO_2)]^-$ (top two spectra) and $[PuO_2(CH_3SO_2)(SO_2)]^-$ (bottom two spectra) with background O_2 in the ion trap for 0.05 s and 0.25 s, as indicated.

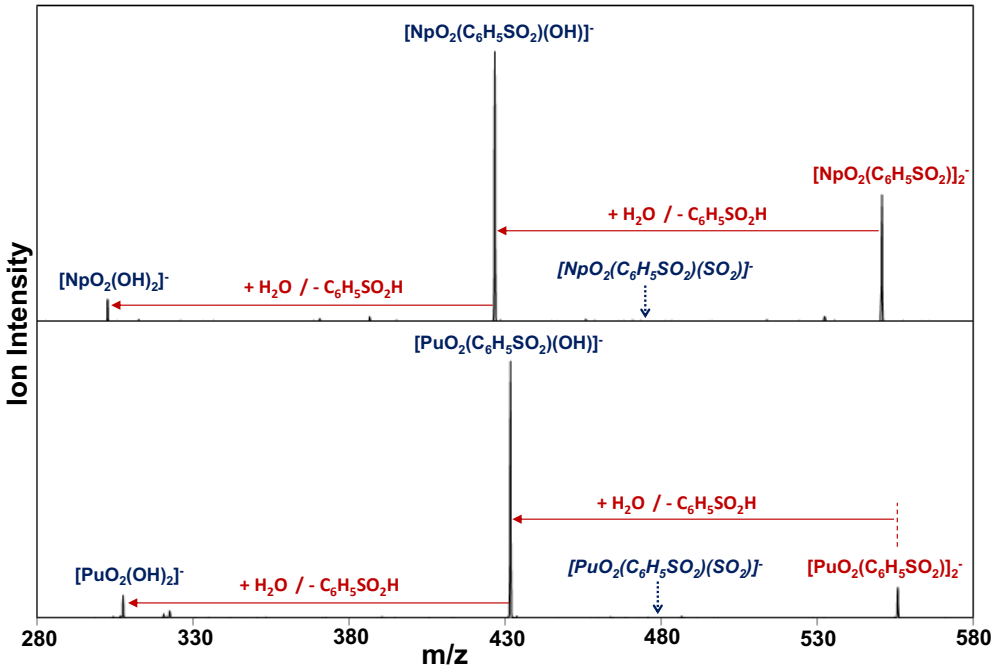

Figure 4. CID mass spectra for $[NpO_2(C_6H_5SO_2)_2]^-$ (top) and $[PuO_2(C_6H_5SO_2)_2]^-$ (bottom). Hydrolysis reactions and products are as indicated. Also indicated are where non-observed ligand fragmentation products in italics would have appeared.

Computed geometries and ground-state electronic configurations

The geometries of the actinyl-SO_2 complexes optimized at the PBE0 level of theory are reported in Table 4 and shown in Figure 5 for exemplary cases. The structures shown for the U(V) complexes in Figure 5, (a)-(d) and (f), are essentially the same as those for the corresponding Np(V) and Pu(V) complexes. The uranyl(VI) complex in Fig. 5 (e) is distinctive, with the corresponding O_2 adducts for neptunyl(V) and plutonyl(V) exhibiting the structure shown in Fig. 5 (g). Most complexes have a linear or nearly linear actinyl unit, with the largest deviation found for $[U^{VI}O_2(CH_3SO_2)(O_2)]^-$ for which the O_{yl}-An-O_{yl} angle is bent to 169.2° from the linear angle of 180°. In most complexes having ionic radical ligands SO_2^- or O_2^-, the spin coupling is low-spin antiferromagnetic; the distinctive exception is high-spin ferromagnetic quintet $[Pu^{V}O_2(CH_3SO_2)(O_2)]^-$ complex.

Table 4. Selected interatomic distances (Å), angles (deg), and asymmetric O_{yl}–An–O_{yl} frequencies (cm^{-1}) of the geometries optimized at the PBE0 level of theory for the complexes, for the most stable oxidation states and dominant spin-multiplicities in the SO-XMS-CASPT2 wave-functions.

Molecule	Multiplicity (2S+1)	r(An-O_{yl})	θ(O_{yl})-An-O_{yl})	ν_{as}(An-O_{yl})	r(An-O_{SO2})	r(An-$O_{SO2\text{-}R}$)	r(An-O_2)/ r(O-O)
$[U^{V}O_2(CH_3SO_2)_2]^-$	2	1.800	180.0	871		2.523	
$[U^{V}O_2(C_6H_5SO_2)_2]^-$	2	1.811	180.0	871		2.532	
$[U^{V}O_2(CH_3SO_2)(SO_2)]^-$	3	1.794	179.7	886	2.550	2.516	
$[U^{V}O_2(C_6H_5SO_2)(SO_2)]^-$	3	1.806	179.6	886	2.554	2.532	
$[U^{VI}O_2(CH_3SO_2)(O_2)]^-$	1	1.782	172.4	915		2.540	2.137/1.417
$[U^{V}O_2(C_6H_5SO_2)(OH)]^-$	2	1.815	169.2	845		2.558	
$[Np^{V}O_2(CH_3SO_2)_2]^-$	3	1.780	180.0	891		2.532	
$[Np^{V}O_2(C_6H_5SO_2)_2]^-$	3	1.771	180.0	892		2.519	
$[Np^{V}O_2(CH_3SO_2)(SO_2)]^-$	2	1.775	179.6	905	2.558	2.523	
$[Np^{V}O_2(C_6H_5SO_2)(SO_2)]^-$	2	1.775	179.7	906	2.546	2.528	
$[Np^{V}O_2(CH_3SO_2)(O_2)]^-$	2	1.778	177.7	895		2.541	2.358/1.310
$[Np^{V}O_2(C_6H_5SO_2)(OH)]^-$	3	1.790	173.9	874		2.566	
$[Pu^{V}O_2(CH_3SO_2)_2]^-$	4	1.759	180.0	901		2.517	
$[Pu^{V}O_2(C_6H_5SO_2)_2]^-$	4	1.759	180.0	902		2.516	
$[Pu^{V}O_2(CH_3SO_2)(SO_2)]^-$	3	1.755	179.8	914	2.542	2.509	
$[Pu^{V}O_2(C_6H_5SO_2)(SO_2)]^-$	3	1.753	177.5	918	2.543	2.533	
$[Pu^{V}O_2(CH_3SO_2)(O_2)]^-$	5	1.767	179.5	909		2.526	2.373/1.304
$[Pu^{V}O_2(C_6H_5SO_2)(OH)]^-$	4	1.769	176.5	888		2.549	

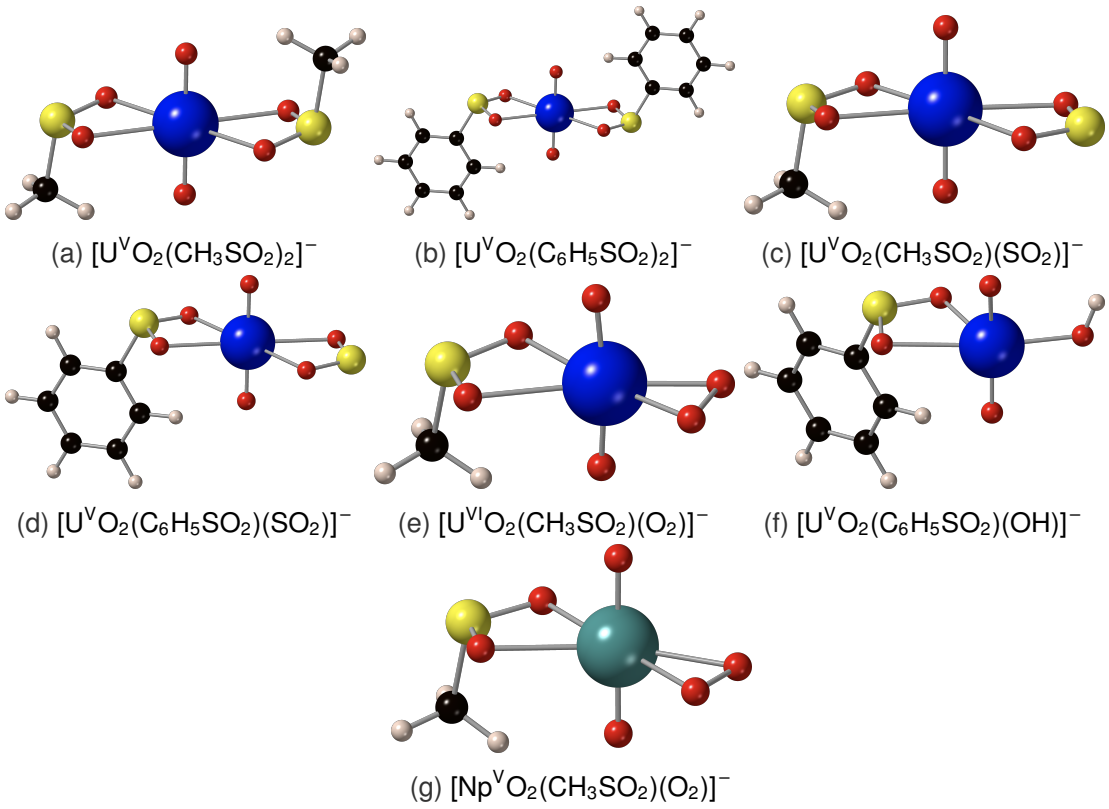

Figure 5. Perspective views of the uranium complexes, and neptunium complex $[Np^{V}O_2(CH_3SO_2)(O_2)]^-$. The structures for the complexes with An = Np and Pu are essentially the same as those shown for An = U in (a), (b), (c), (d) and (f). The structure for An = Pu is essentially the same as that shown for An = Np in (g).

Most of the uranyl complexes contain pentavalent U, with the exception of $[U^{VI}O_2(CH_3SO_2)(O_2)]^-$, which is closed-shell singlet U(VI) coordinated by a bidentate peroxide O_2^{2-} and a sulfinate $CH_3SO_2^-$. The O-O bond length of 1.417 Å in this U(VI) complex is consistent with that of a peroxide, and the uranyl asymmetric stretch frequency is blue shifted by about 30 to 40 cm^{-1} with respect to the U(V) complexes. For uranyl complexes that differ only by swapping the $CH_3SO_2^{\bullet}$ and $C_6H_5SO_2^{\bullet}$ ligands, the U-$O_{SO2\text{-}R}$ distances are similar to within <0.02 Å, which confirms the expected similar uranium-ligand bonding for different sulfinates.

All of the considered neptunyl and plutonyl complexes have a pentavalent actinide center. The alternative $[AnO_2(CH_3SO_2)(O_2)]^-$ peroxide with electronic configurations corresponding to An(VI) were found to be unstable, converging instead to An(V). In the $[An^{V}O_2(CH_3SO_2)(O_2)]^-$, the dioxo ligand is a superoxide O_2^- with accordingly short O-O distances (1.310 Å for An = Np; 1.304 Å for An = Pu). The $[An^{V}O_2(CH_3SO_2)_2]^-$, $[An^{V}O_2(C_6H_5SO_2)_2]^-$, and

$[An^{V}O_2(C_6H_5SO_2)(OH)]^-$ complexes have high-spin ground-states—triplet for An = Np and quartet for An = Pu—that correspond respectively to two and three unpaired electrons localized in the non-bonding actinide $5f_\varphi$ and $5f_\delta$ orbitals.

The nature of the electronic ground states of the complexes with a O_2^- superoxo or SO_2^- radical depends on the actinide center, as revealed by the results in Table 5 and by the NSOs drawn in Figure 6, together with their spin occupations. For the U(V), Np(V) and Pu(V) complexes there are respectively one, two and three spin-parallel non-bonding 5f electrons, designated as $f^{1,\alpha}$, $f^{2,\alpha}$ and $f^{3,\alpha}$. The radical ligand electron can then exhibit parallel spin, designated L^α, to yield a high-spin ferromagnetic (FM) complex, or an anti-parallel spin, L^β, to yield a low-spin anti-FM (AFM) complex. Complexes $[U^{V}O_2(CH_3SO_2)(SO_2)]^-$ and $[U^{V}O_2(C_6H_5SO_2)(SO_2)]^-$ have GSs dominated by triplet spin-free state that corresponds to FM coupling. However, the AFM singlet states are only 13 cm^{-1} high energy, which is smaller than the computational uncertainty and indicates only minor magnetic coupling. In the corresponding neptunium and plutonium complexes the GS is dominated by AFM coupling to yield doublet for An = Np and triplet for An = Pu (see Figure 6 (a), (b), and (d)). The high-spin FM states lie only about 240 cm^{-1} (2.9 kJ mol^{-1}) higher for An = Np, but 1590-2000 cm^{-1} higher for An = Pu. The results for complexes with an O_2^- superoxide radical ligand are particularly intriguing. For $[NpO_2(CH_3SO_2)(O_2)]^-$ the GS is again AFM doublet, in which the two spins localized on neptunyl are antiferromagnetically coupled with the superoxide radical spin; the FM quartet state lies 1065 cm^{-1} higher energy. However, for $[PuO_2(CH_3SO_2)(O_2)]^-$ the GS is FM quintet with the AFM triplet state only 193 cm^{-1} higher energy. Thus, the GS of the Pu^{V} complex with an SO_2^- ligand is low-spin AFM triplet, whereas with an O_2^- ligand it is high-spin FM quintet; the energy shifts from favoring AFM by 1586 cm^{-1} to favoring FM by 193 cm^{-1}. The latter energy is sufficiently small that the actual GS could be AFM, with the energies at this level of accuracy possibly skewed due to strong interplay between electron correlation effects and spin-orbit interactions. Notably, AFM coupling was similarly reported for $[AnO_3(NO_3)_2]^-$ [36] and AnS_2^+ complexes.[37] Our QTAIM analysis of the bonds in $[U^{V}O_2(CH_3SO_2)(SO_2)]^-$ and $[Np^{V}O_2(CH_3SO_2)(SO_2)]^-$, summarized in Table 6, reveal that the U^{V}-SO_2 bond is slightly more covalent than the Np^{V}-SO_2, which evidently favors FM coupling in the former versus AFM coupling in the latter.

Table 5. Energy relative to the electronic ground-state (GS) of the lowest-lying state with different spin. The GS configuration is characterized as $f^{n,S}L^{S}$ where S = α or β is the spin of non-bonding electrons in actinide 5f and radical ligand orbitals. Energy gap ΔE between high-spin (ferromagnetic, FM) and low-spin (anti-ferromagnetic, AFM) is the coupling between 5f and ligand electrons.

Molecule	GS-mult	Config.	lowest alternate spin state (alt.)	ΔE[GS→alt.] (cm^{-1}/ kJ mol^{-1})
$[U^{V}O_2(CH_3SO_2)(SO_2)]^-$	triplet (FM)	$f^{1,\alpha}L^{\alpha}$	singlet (AFM)	13 / 0.15
$[U^{V}O_2(C_6H_5SO_2)(SO_2)]^-$	triplet (FM)	$f^{1,\alpha}L^{\alpha}$	singlet (AFM)	13 / 0.15
$[Np^{V}O_2(CH_3SO_2)(SO_2)]^-$	doublet (AFM)	$f^{2,\alpha}L^{\beta}$	quartet (FM)	239 / 2.9
$[Np^{V}O_2(C_6H_5SO_2)(SO_2)]^-$	doublet (AFM)	$f^{2,\alpha}L^{\beta}$	quartet (FM)	241 / 2.9
$[Np^{V}O_2(CH_3SO_2)(O_2)]^-$	doublet (AFM)	$f^{2,\alpha}L^{\beta}$	quartet (FM)	1065 / 12.7
$[Pu^{V}O_2(CH_3SO_2)(SO_2)]^-$	triplet (AFM)	$f^{3,\alpha}L^{\beta}$	quintet (FM)	1586 / 19.0
$[Pu^{V}O_2(C_6H_5SO_2)(SO_2)]^-$	triplet (AFM)	$f^{3,\alpha}L^{\beta}$	quintet (FM)	2000 / 23.9
$[Pu^{V}O_2(CH_3SO_2)(O_2)]^-$	quintet (FM)	$f^{3,\alpha}L^{\alpha}$	triplet (AFM)	193 / 2.3

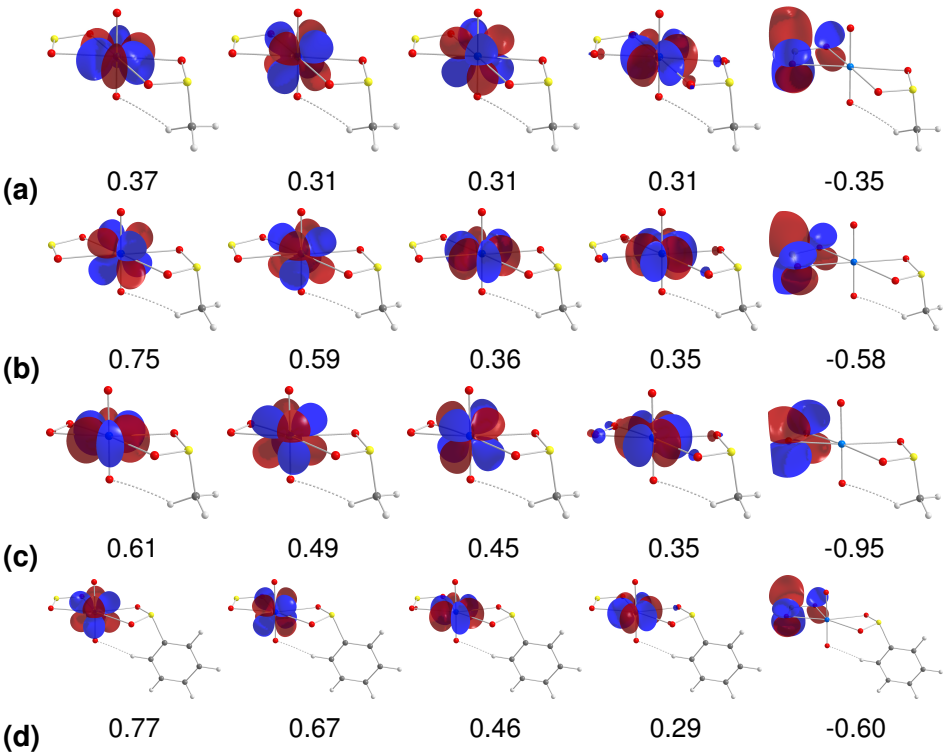

Figure 6. Selected Natural Spin Orbitals NSOs along the z-O_{yl} direction for SO ground state of (a) $[Np^{V}O_2(CH_3SO_2)(SO_2)]^-$; (b) $[Pu^{V}O_2(CH_3SO_2)(SO_2)]^-$; (c) $[Np^{V}O_2(CH_3SO_2)(O_2)]^-$; (d) $[Pu^{V}O_2(C_6H_5SO_2)(SO_2)]^-$, with indicated occupation numbers n_z. Isosurface values are ±0.03 au.

Table 6. QTAIM characteristics of the An–SO_2 bond critical point (BCP) in ferromagnetically coupled $[U^{V}O_2(CH_3SO_2)(SO_2)]^-$ and anti-ferromagnetically coupled $[Np^{V}O_2(CH_3SO_2)(SO_2)]^-$. ρ_b is the density at the BCP, $\nabla\rho_b$ is the Laplacian of the density, and DI(An-L) is the delocalization index.

BCP	$[U^{V}O_2(CH_3SO_2)(SO_2)]^-$	$[Np^{V}O_2(CH_3SO_2)(SO_2)]^-$
ρ_b/ e^3 a_0^{-1}	0.045	0.044
$\nabla\rho_b$ / e a_0^{-5}	0.183	0.181
DI(An-L)	0.271	0.267

Computed reaction energies and comparison with experimental observations

Reaction enthalpies computed for reactions (8) to (11) at various levels of theory—B3LYP, PBE0, CASSCF, XMS-CASPT2 (PT2) and SO-XMS-CASPT2 with SO (PT2+SO)—are in Table 7. Energies from DFT using B3LYP or PBE0 functional deviate from CASPT2 values by up to ca. 80 kJ mol^{-1}. The inaccuracies of these functionals for energetics is probably due to self-interaction errors, combined with the lack of treatment the multireference character of the wave-functions. For uranium, spin-orbit coupling is negligible for reactions (8), (10) and (11) which have U(V) in both reactants and products. However, for reaction (9)—oxidation from open-shell $5f^1$ U(V) to closed-shell $5f^0$ U(VI)—stabilization of the reactant due to SO coupling diminishes the exothermicity by 31.5 kJ mol^{-1}. As the trends in reaction energies are the same for all employed levels of theory, we focus on the energies obtained using CASPT2+SO.

Table 7. Reaction enthalpies ΔH_r at 298.15 K in kJ mol^{-1} for reactions (8) to (11) computed at various levels of theory. The spin-orbit contribution (Δ) is in parenthesis.

Reaction	B3LYP	B3LYP[9]	PBE0	CASSCF	PT2	PT2+SO (Δ)
			Uranyl			
(8)	172.8	162.0	196.2	143.5	178.6	177.8 (-0.8)
(9)	-48.0	-18.0	-33.3	52.0	-122.7	-91.2 (31.5)
(10)	206.5	N/A	229.1	178.7	230.6	228.5 (-2.1)
(11)	119.8	N/A	117.7	144.1	145.9	145.9 (0.0)
			Neptunyl			
(8)	N/A	N/A	194.9	142.0	176.1	174.8 (-1.3)
(9)	N/A	N/A	-10.0	-54.0	-47.5	-36.8 (10.7)
(10)	N/A	N/A	226.7	178.7	224.2	225.7 (1.5)
(11)	N/A	N/A	125.8	151.7	149.8	148.7 (-1.9)
			Plutonyl			
(8)	N/A	N/A	193.4	141.6	162.0	165.3 (3.3)
(9)	N/A	N/A	27.6	-52.8	-24.5	0.9 (25.4)
(10)	N/A	N/A	241.1	186.5	206.0	218.9 (12.9)
(11)	N/A	N/A	135.4	158.1	158.1	155.3 (-2.8)

It was previously reported that CID reaction (8) occurs for An = U, and it was shown here (Fig. 2) that is also occurs for An = Np and Pu. The computed reaction (8) energies are similar for all three An, to within 10 kJ mol^{-1}, reflecting that they all correspond to cleavage of a CH_3-$SO_2^{\bullet}$ bond to convert a $CH_3SO_2^-$ ligand to a SO_2^- ligand. Referring to Table 4, the An-$O_{SO2\text{-}CH3}$ and An-O_{SO2} distances differ by only ca. 0.03 Å, indicating similar actinide-ligand bonding in the reactants and products. The substantial endothermicities for reaction (8) should thus be dominated by CH_3-SO_2 bond dissociation energy (BDE). Accordingly, the computed energies for reaction (8), 165-178 kJ mol^{-1} are only slightly smaller than the BDE[CH_3-SO_2^-] reported in Table 2 for reaction (3a) (i.e., BDE = 198 kJ mol^{-1} using CCSD(T)).

Spontaneous reaction (9) was previously reported for An = U, and was observed here for An = Np and Pu. The results in Table 7 indicate that this reaction is substantially exothermic for An = U, moderately exothermic for An = Np, and nearly thermoneutral for An = Pu. For the last case the computed ΔH_r of only 0.9 kJ mol^{-1} is within the available energy at the reaction temperature of ~300 K, such that observed reaction (9) is computationally predicted to occur for

all three An. As noted above, the products of reaction (9) are U(VI) peroxide but Np(V) and Pu(V) superoxides. The standard An(VI→V) reduction potentials, E^0[VI/V], provide estimates of the relative energies for reaction (9) if the replaced SO_2^- ligand is a O_2^{2-} peroxide, with resultant oxidation from An(V) to An(VI). Compared with oxidation of U(V) to U(VI), that of Np(V) to Np(VI) is ca. 104 kJ mol^{-1} less favorable and that of Pu(V) to Pu(VI) is ca. 82 kJ mol^{-1} less favorable.[11] As a result of their higher reduction potentials, E^0[VI/V], the energetically favored reactions and products are An(V) superoxides, rather than An(VI) peroxides, for An = Np and Pu.

A starting premise of this investigation was that the R-SO_2 bond strength would exert control over the observed CID fragmentation. Indeed, the CID results above (Fig. 4) show that reaction (10) is not observed for An = Np and Pu (An = U was not studied), whereas reaction (8) is. The results reported in Table 2 indicate that BDE[C_6H_5-SO_2^-] is ca. 78 kJ mol^{-1} greater than BDE[CH_3-SO_2] (using the MP2(CBS) values). For comparison, the computed energies for reaction (10) are ca. 50 kJ mol^{-1} higher than for reaction (8), a difference that can be attributed primarily to the 78 kJ mol^{-1} stronger R-SO_2 bond energy in benzenesulfinate. The experimental and computational results thus demonstrate that an increase in the sulfinate C-S bond energy essentially shuts off the ligand fragmentation pathway upon changing the ligand from $CH_3SO_2^-$ to $C_6H_5SO_2^-$.

The CID process that was observed for $[AnO_2(C_6H_5SO_2)_2]^-$ (An = Np, Pu) was not simple unimolecular ligand fragmentation reaction (10) but instead bimolecular hydrolysis reaction (11). Compared with reaction (10), the computed energies for observed reaction (11) are 77 kJ mol^{-1} and 64 kJ mol^{-1} lower for An = Np and Pu, respectively. The energies required for reaction (11), ca. 150 kJ mol^{-1}, are slightly lower than those for observed reaction (8), and are thus well within the energy available to the reaction system under these CID conditions. For completeness, we note that simple unimolecular neutral ligand elimination absent a reactive water molecule, reaction (12), was not observed. This process would result in the indicated reduction of the actinide center from An(V) to An(IV). Observed hydrolytic ligand elimination reaction (11) retains the An(V) oxidation state, as well as a non-radical sulfinate anion, which evidently favors this process over reaction (12). Another reasonable possibility is CID reaction (13), elimination of a sulfinate anion. As the instrumental low-mass CID cutoff—ca. 150 m/z for $[An^VO_2(C_6H_5SO_2)_2]^-$—is slightly above the ligand mass of 141 Da, reaction (13) would not have

been detected in our experiments. Although reaction (13) may have occurred, the inability to observe it does not whatsoever invalidate the certain occurrence of reaction (11), nor interpretations associated with that reality.

$$[An^{V}O_2(C_6H_5SO_2)_2]^- \rightarrow [An^{IV}O_2(C_6H_5SO_2)]^- + C_6H_5SO_2^{\bullet} \quad (12)$$

$$[An^{V}O_2(C_6H_5SO_2)_2]^- \rightarrow [An^{V}O_2(C_6H_5SO_2)] + C_6H_5SO_2^- \quad (13)$$

Conclusions

DFT (PBE0), MP2, and CCSD(T) computations show that the lowest energy structures of bare neutral and anionic sulfinates are different. The neutrals exhibit C-O-S-O connectivity in $CH_3OSO^{\bullet}$ and $C_6H_5OSO^{\bullet}$, whereas the anions exhibit C-SO_2 connectivity in $CH_3SO_2^-$ and $C_6H_5SO_2^-$, the latter being the relevant structures when the moieties are ligands complexed to electropositive metal centers such as actinides. The computed bond dissociation energies (BDEs) confirm the empirically based prediction that BDE[C_6H_5-SO_2^-] is substantially greater than BDE[CH_3-SO_2^-].

Collision induced dissociation (CID) of neptunyl(V) and plutonyl(V) sulfinate complexes resulted in different fragmentation pathways that reflect the strength of the C-S bond in the ligand. CID of $[An^{V}O_2(CH_3SO_2)_2]^-$ resulted in C-S bond cleavage with CH_3 elimination to afford $[An^{V}O_2(CH_3SO_2)(SO_2)]^-$ for An = Np and Pu. CID of the corresponding $[An^{V}O_2(C_6H_5SO_2)_2]^-$ complexes contrastingly resulted in reaction with a water molecule to produce $C_6H_5SO_2H$ and $[An^{V}O_2(CH_3SO_2)(OH)]^-$. Complete active space computations show that the difference in chemistry for the two sulfinate ligands—C-S cleavage for $CH_3SO_2^{\bullet}$ versus ligand elimination for $C_6H_5SO_2^{\bullet}$—stems from the disparate C-S bond energies identified for the bare sulfinate anions. The results demonstrate rational control of decomposition chemistry, which might be applicable to condensed phase systems. For example, thermal decomposition of an actinide methanesulfinate could be a source of sulfur dioxide materials whereas the corresponding benzenesulfinate should be more prone to react with ambient water to yield hydroxides. More generally, methanesulfinate is expected to be a better source of radical $C^{\bullet}$ for carbon-carbon coupling.

The two $[An^{V}O_2(CH_3SO_2)(SO_2)]^-$ (An = Np, Pu) generated by CID reacted with O_2 in an ion trap to displace SO_2 and yield $[AnO_2(CH_3SO_2)(O_2)]^-$ where the oxidation state of the actinide may reasonably be An(V) with a superoxide O_2^- ligand, or An(VI) with a peroxide O_2^{2-} ligand. A similar SO_2/O_2 exchange reaction was previously reported for $[U^{V}O_2(CH_3SO_2)(SO_2)]^-$ giving

$[U^{VI}O_2(CH_3SO_2)(O_2)]^-$, where oxidation of U(V) to U(VI) peroxide was indicated by computations. Computations here show that for An = Np and Pu, the complexes are instead superoxides $[An^{V}O_2(CH_3SO_2)(O_2)]^-$. The different chemistry of uranium versus neptunium and plutonium with the redox-active O_2 ligand reflects the relatively easier oxidation from U(V) to U(VI). This is a case where essential actinide behavior is revealed in small gas-phase complexes, demonstrating the utility of such systems and approaches for elucidating chemistry with only very small amounts of materials such as may be available for heavier and scarcer actinide and transactinide elements.

SUPPORTING INFORMATION

ESI mass spectra for actinyl methanesulfinate solutions. Natural Spin Orbitals for $[UO_2(CH_3SO_2)(SO_2)]^-$ and $[NpO_2(C_6H_5SO_2)(SO_2)]^-$. The input and output files of the quantum chemical calculations presented in this study are openly available in Zenodo at DOI: 10.5281/zenodo.3600559.

AUTHOR INFORMATION

Corresponding Authors

Valérie Vallet: valerie.vallet@univ-lille.fr

John K. Gibson: jkgibson@lbl.gov

Present Addresses

Yu Gong, Department of Radiochemistry, Shanghai Institute of Applied Physics, Chinese Academy of Sciences, Shanghai 201800, China

ACKNOWLEDGEMENTS

The experimental work was fully supported by the U.S. Department of Energy (DOE), Office of Science, Office of Basic Energy Sciences, Chemical Sciences, Geosciences, and Biosciences Division, Heavy Element Chemistry Program, at Lawrence Berkeley National Laboratory under Contract DE-AC02-05CH1123 (YG, JKG). The theoretical work has been supported by the French government through the Program ”Investissement d’avenir” (LABEX CaPPA/ANR-11-LABX-0005-01 and I-SITE ULNE/ANR-16-IDEX-0004 ULNE), as well as by the Ministry of Higher Education and Research, Hauts de France council, and European Regional Development Fund (ERDF) through the Contrat de Projets Etat-Region (CPER CLIMIBIO).

REFERENCES

(1) Yuan, K. D.; Soule, J. F.; Doucet, H. Functionalization of C-H Bonds via Metal-Catalyzed Desulfitative Coupling: An Alternative Tool for Access to Aryl- or Alkyl-Substituted (Hetero)arenes. *Acs Catal* 2015, *5*, 978-991.

(2) O'Hair, R. A. J.; Rijs, N. J. Gas Phase Studies of the Pesci Decarboxylation Reaction: Synthesis, Structure, and Unimolecular and Bimolecular Reactivity of Organometallic Ions. *Accounts Chem Res* 2015, *48*, 329-340.

(3) O'Hair, R. A. J. The 3D quadrupole ion trap mass spectrometer as a complete chemical laboratory for fundamental gas-phase studies of metal mediated chemistry. *Chem Commun* 2006, 1469-1481.

(4) Altuntas, E.; Winter, A.; Baumgaertel, A.; Paulus, R. M.; Ulbricht, C.; Crecelius, A. C.; Risch, N.; Schubert, U. S. Determination of the relative ligand-binding strengths in heteroleptic IrIII complexes by ESI-Q-TOF tandem mass spectrometry. *J Mass Spectrom* 2012, *47*, 34-40.

(5) Serra, D.; Moret, M. E.; Chen, P. Transmetalation of Methyl Groups Supported by Pt-II-Au-I Bonds in the Gas Phase, in Silico, and in Solution. *J Am Chem Soc* 2011, *133*, 8914-8926.

(6) Gong, Y.; Vallet, V.; Michelini, M. D.; Rios, D.; Gibson, J. K. Activation of Gas-Phase Uranyl: From an Oxo to a Nitrido Complex. *J Phys Chem A* 2014, *118*, 325-330.

(7) Sraj, L. O.; Khairallah, G. N.; da Silva, G.; O'Hair, R. A. J. Who Wins: Pesci, Peters, or Deacon? Intrinsic Reactivity Orders for Organocuprate Formation via Ligand Decomposition. *Organometallics* 2012, *31*, 1801-1807.

(8) Wang, Z. L.; Yang, Y.; Donnelly, P. S.; Canty, A. J.; O'Hair, R. A. J. Desulfination versus decarboxylation as a means of generating three-and five-coordinate organopalladium complexes [(phen)(n)Pd(C6H5)](+) (n=1 and 2) to study their fundamental bimolecular reactivity. *J Organomet Chem* 2019, *882*, 42-49.

(9) Gong, Y.; Gibson, J. K. Formation and Characterization of the Uranyl--SO2 Complex, UO2(CH3SO2)(SO2)-. *J. Phys. Chem. A* 2013, *117*, 783-787.

(10) Baker, L.; Schnizlein, J. G.; Bingle, J. D. Ignition of Uranium. *J Nucl Mater* 1966, *20*, 22-+.

(11) Edelstein, N. M.; Fuger, J.; Katz, J. J.; Morss, L. R.: Summary and Comparison of Properties of the Actinide and Transactinide Elements. In *The Chemistry of the Actinide and Transactinide Elements*; Third ed.; Morss, L. R., Edelstein, N. M., Fuger, J., Eds.; Springer: Dordrecht, The Netherlands, 2006; Vol. 3; pp 1753-1835.

(12) Hammond, G. S. A Correlation of Reaction Rates. *J Am Chem Soc* 1955, *77*, 334-338.

(13) Lias, S. G.; Bartmess, J. E.; Liebman, J. F.; Holmes, J. L.; Levin, R. D.; Mallard, W. G. Gas-Phase Ion and Neutral Thermochemistry. *J Phys Chem Ref Data* 1988, *17*, 1-861.

(14) Dunning, J., T. H. Gaussian basis sets for use in correlated molecular calculations. I. The atoms boron through neon and hydrogen. *J. Chem. Phys.* 1989, *90*, 1007-1023.

(15) Küchle, W.; Dolg, M.; Stoll, H.; Preuss, H. Energy-adjusted pseudopotentials for the actinides. Parameter sets and test calculations for thorium and thorium monoxide. *J. Chem. Phys.* 1994, *100*, 7535-7542.

(16) Cao, X.; Dolg, M. Segmented contraction scheme for small-core actinide pseudopotential basis sets. *J. Mol. Struct. (Theochem)* 2004, *673*, 203-209.

(17) H.-J. Werner, P. J. K., G. Knizia, F. R. Manby, M. Schu¨tz, P. Celani, W. Gy¨orffy, D. Kats,; T. Korona, R. L., A. Mitrushenkov, G. Rauhut, K. R. Shamasundar, T. B. Adler, R. D. Amos,; A. Bernhardsson, A. B., D. L. Cooper, M. J. O. Deegan, A. J. Dobbyn, F. Eckert, E. Goll,; C. Hampel, A. H., G. Hetzer, T. Hrenar, G. Jansen, C. K ¨oppl, Y. Liu, A. W. Lloyd, R. A. Mata, A. J. May, S. J. McNicholas, W. Meyer, M. E. Mura, A. Nicklass, D. P. O'Neill, P. Palmieri, K. Pflüger, R. Pitzer, M. Reiher, T. Shiozaki, H. Stoll, A. J. Stone, R. Tarroni, T. Thorsteinsson, and M. Wang: MOLPRO, version~2015.1, a package of ab initio programs. "Cardiff, UK", 2015.

(18) Karton, A.; Martin, J. M. L. Comment on: "Estimating the Hartree-Fock limit from finite basis set calculations" [Jensen F (2005) Theor Chem Acc 113, 267]. *Theor Chem Acc* 2006, *115*, 330-333.

(19) Feller, D.; Peterson, K. A.; Dixon, D. A. A survey of factors contributing to accurate theoretical predictions of atomization energies and molecular structures. *J Chem Phys* 2008, *129*.

(20) Feller, D.; Peterson, K. A.; Hill, J. G. On the effectiveness of CCSD(T) complete basis set extrapolations for atomization energies. *J Chem Phys* 2011, *135*.

(21) Aquilante, F.; Autschbach, J.; Carlson, R. K.; Chibotaru, L. F.; Delcey, M. G.; De Vico, L.; Fdez. Galván, I.; Ferré, N.; Frutos, L. M.; Gagliardi, L.; Garavelli, M.; Giussani, A.; Hoyer, C. E.; Li Manni, G.; Lischka, H.;

Ma, D.; Malmqvist, P. Å.; Müller, T.; Nenov, A.; Olivucci, M.; Pedersen, T. B.; Peng, D.; Plasser, F.; Pritchard, B.; Reiher, M.; Rivalta, I.; Schapiro, I.; Segarra-Martí, J.; Stenrup, M.; Truhlar, D. G.; Ungur, L.; Valentini, A.; Vancoillie, S.; Veryazov, V.; Vysotskiy, V. P.; Weingart, O.; Zapata, F.; Lindh, R. Molcas 8: New capabilities for multiconfigurational quantum chemical calculations across the periodic table. *J. Comput. Chem.* 2016, *37*, 506-541.

(22) Wolf, A.; Reiher, M.; Hess, B. A. The generalized Douglas--Kroll transformation. *J. Chem. Phys.* 2002, *117*, 9215-9226.

(23) Roos, B. O.; Lindh, R.; Malmqvist, P.-Å.; Veryazov, V.; Widmark, P.-O. Main group atoms and dimers studied with a new relativistic ANO basis set. *J. Phys. Chem. A* 2004, *108*, 2851-2858.

(24) Roos, B. O.; Lindh, R.; Malmqvist, P.-Å.; Veryazov, V.; Widmark, P.-O. New relativistic ANO basis sets for actinide atoms. *Chem. Phys. Lett.* 2005, *409*, 295-299.

(25) Shiozaki, T.; Győrffy, W.; Celani, P.; Werner, H.-J. Communication: Extended multi-state complete active space second-order perturbation theory: Energy and nuclear gradients. *J. Chem. Phys.* 2011, *135*, 081106.

(26) Malmqvist, P.-Å.; Roos, B. O.; Schimmelpfennig, B. The restricted active space (RAS) state interaction approach with spin-orbit coupling. *Chem. Phys. Lett* 2002, *357*, 230-240.

(27) Schimmelpfennig, B.: AMFI, an Atomic Mean-Field Integral program. 1996.

(28) Gendron, F.; Pritchard, B.; Bolvin, H.; Autschbach, J. Magnetic Resonance Properties of Actinyl Carbonate Complexes and Plutonyl(VI)-tris-nitrate. *Inorg. Chem.* 2014, *53*, 8577-8592.

(29) Gendron, F.; Bolvin, H.; Autschbach, J.: Complete Active Space Wavefunction-Based Analysis of Magnetization and Electronic Structure. In *Topics in Organometallic Chemistr*; Springer: Berlin, Heidelberg, 2018; pp 1--36.

(30) Keith, T. A.: AIMAll (version 14.11.23), Todd A. Keith, TK Gristmill Software: Overland Park KS, 2014. \urlhttp://aim.tkgristmill.com.

(31) Rios, D.; Rutkowski, P. X.; Shuh, D. K.; Bray, T. H.; Gibson, J. K.; Van Stipdonk, M. J. Electron transfer dissociation of dipositive uranyl and plutonyl coordination complexes. *J Mass Spectrom* 2011, *46*, 1247-1254.

(32) Gronert, S. Estimation of effective ion temperatures in a quadrupole ion trap. *J Am Soc Mass Spectr* 1998, *9*, 845-848.

(33) Rios, D.; Michelini, M. C.; Lucena, A. F.; Marcalo, J.; Bray, T. H.; Gibson, J. K. Gas-Phase Uranyl, Neptunyl, and Plutonyl: Hydration and Oxidation Studied by Experiment and Theory. *Inorg Chem* 2012, *51*, 6603-6614.

(34) Rutkowski, P. X.; Michelini, M. C.; Bray, T. H.; Russo, N.; Marcalo, J.; Gibson, J. K. Hydration of gas-phase ytterbium ion complexes studied by experiment and theory. *Theor Chem Acc* 2011, *129*, 575-592.

(35) Li, X.; Meng, L.; Zeng, Y.; Zheng, S. Isomerizations of CH3SO2: Quantum Chemistry and Topological Study. *2010* Chin. J. Chem., *28*, 896-900.

(36) Dau, P. D.; Maurice, R.; Renault, E.; Gibson, J. K. Heptavalent Neptunium in a Gas-Phase Complex: (Np(VII)O3+)(NO_3^-)2. *Inorg. Chem.* 2016, *55*, 9830-9837.

(37) Lucena, A. F.; Bandeira, N. A. G.; Pereira, C. C. L.; Gibson, J. K.; Marçalo, J. Synthesis, structure and bonding of actinide disulphide dications in the gas phase. *Phys. Chem. Chem. Phys.* 2017, *19*, 10685-10694.

Table of Contents Graphic